Electromagnetic Emission-aware Machine Learning Enabled Scheduling Framework for Unmanned Aerial Vehicles

Electromagnetic Emission-aware Machine Learning Enabled Scheduling Framework for Unmanned Aerial Vehicles

Muhammad Ali Jamshed, Ali Nauman, Ayman A. Althuwayb, Haris Pervaiz, Sung Won Kim

Abstract

Recently, there has been a notable increase in the number of User Proximity Wireless Devices (UPWD). This growth has significantly raised users' exposure to Electromagnetic Field (EMF), potentially leading to various physiological effects. The use of Non-Terrestrial Networks (NTN) has emerged as an optimistic solution to improve wireless coverage in rural areas. NTN mainly consist of satellites, with High Altitude Platform Stations (HAPS) and Unmanned Aerial Vehicles (UAV) considered special use cases. It is well established that optimizing exposure over time (Dose), rather than dealing with a fixed value, plays a crucial role in reducing uplink EMF exposure levels. In this paper, for the first time, we showcase that the combined use of UAV and the Dose metric can help keep the regulated uplink EMF exposure level well below the required threshold. This paper employs a combination of Non-Orthogonal Multiple Access (NOMA), UAV technology, Machine Learning (ML), and the Dose metric to optimize EMF exposure in the uplink of wireless communication systems. The ML based technique consists of a combination of k-medoids-based clustering and Silhouette analysis. To further reduce uplink EMF exposure, a power allocation policy is developed by transforming a non-convex problem into a convex one for solution. The numerical results indicate that the proposed scheme, which integrates NOMA, NTN, and ML, achieves at least a 89% reduction in EMF contrast to existing methods.

Index Terms

Electromagnetic Field (EMF), Non-Orthogonal Multiple Access (NOMA), Machine Learning (ML), Exposure Dose, Unmanned Aerial Vehicle (UAV).

I. Introduction

RECENTLY, the popularity of wireless personal devices has significantly increased, leading to an exponential rise in their number and usage [1]. As these devices typically emit non-ionizing Electromagnetic Field (EMF) radiation, the use of User Proximity Wireless Devices (UPWD) has been associated with potential negative impacts on human physiology. Although the current evidence on the immediate health impacts of EMF exposure is inconclusive, it is important to note that the World Health Organization (WHO) and the International Agency for Research on Cancer (IARC) have classified EMF radiation from UPWD as Group 2B, indicating limited or no evidence of carcinogenicity. While the Federal Communication Commission (FCC) and International Commission on Non-Ionizing Radiation Protection (ICNIRP) have established guidelines on the maximum allowable absorbed EMF limit, the FCC consumer guidelines state that "FCC approval does not necessarily indicate the precise extent of EMF exposure that consumers may encounter during the normal use of a device" [2]. Consequently, the proliferation of EMF radiation in the 5G era has the potential to amplify long-term health risks associated with EMF exposure [3]. We believe that there are untapped opportunities and solutions that can be utilized to optimize EMF exposure and ensure the enduring sustainability of wireless communication systems.

A significant advancement in recent years for the evolution of next-generation communication systems is the rise of Non-Terrestrial Networks (NTN). NTN represents a transformative phase in connectivity as it extends beyond Earth's surface [4]. The release of 3rd Generation Partnership Project (3GPP) Release 17 signifies a major milestone in integrating NTN and Terrestrial Network (TN). NTN encompass a diverse array of pioneering communication systems that operate beyond the constraints of traditional terrestrial infrastructure. They present possibilities for worldwide connectivity via the internet, the Internet of Things (IoT), disaster preparedness, navigation systems, remote access, and numerous scientific pursuits. According to 3GPP guidelines, NTN typically consists of satellites, while High Altitude Platform Stations (HAPS) and Unmanned Aerial Vehicles (UAV) are regarded as special use cases. It is perhaps less documented how the special use case of NTN, specifically UAV, can significantly reduce EMF exposure, particularly in dense urban scenarios, where the likelihood of Line-of-Sight (LoS) can be enhanced by utilizing UAV [5], [6].

M. A. Jamshed is with the College of Science and Engineering, University of Glasgow, G12 8QQ, UK (email: muhammadali.jamshed@glasgow.ac.uk).

Corresponding Author: A. Nauman is with the School of Computer Science and Engineering, Yeungnam University, Gyeongsan-si, Republic of Korea (email:anauman@ynu.ac.kr)

Co-corresponding Author: A. A. Althuwayb is with the Electrical Engineering Department, College of Engineering, Jouf University, Sakaka, Aljouf 72388, Kingdom of Saudi Arabia (e-mail: aaalthuwayb@ju.edu.sa)

H. Pervaiz is with the School of Computer Science and Electronic Engineering, University of Essex, UK (email: haris.pervaiz@essex.ac.uk)

Sung Won Kim is with the School of Computer Science and Engineering, Yeungnam University, Gyeongsan-si, Republic of Korea (email: swon@yu.ac.kr)

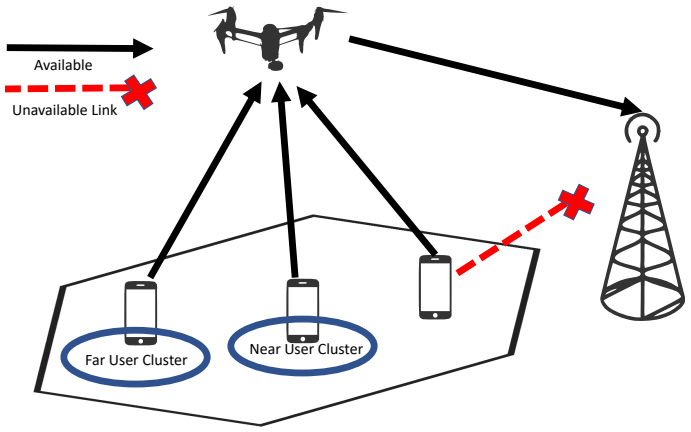

Figure 1: A high-level exemplification of the system model developed to explain the working of the proposed mechanism.

Earlier generations of mobile communication technologies predominantly employed Orthogonal Multiple Access (OMA) methods such as Time-Division Multiple Access (TDMA) and Orthogonal Frequency Division Multiple Access (OFDMA) to multiplex users. Nevertheless, the emergence of Non-orthogonal Multiple Access (NOMA) has brought forward an innovative method for the next era of cellular communication. NOMA encompasses two primary variants: Power Domain NOMA (PD-NOMA) and Code-Domain NOMA (CD-NOMA), with CD-NOMA incorporating techniques like Sparse Code Multiple Access (SCMA) [7]. This discussion will focus on PD-NOMA, which exploits differences in channel gains among users to assign them to the same subcarrier with varying transmission powers. This innovative strategy enables concurrent scheduling of a larger number of users [8], [9]. Unlike OMA, NOMA demonstrates the capability to support a greater user base, thereby enhancing spectral efficiency. Additionally, the characteristics of PD-NOMA present intriguing possibilities for reducing EMF exposure while maintaining Quality-of-Service (QoS).

Enhanced Mobile Broadband (eMBB) has paved the way for ultra-high-definition streaming and augmented/virtual reality (AR/VR) experiences in 5G. The aspirations for 6G extend performance expectations across a broad spectrum of innovative applications [10]. These applications have escalated the demand for data rates, consequently increasing power consumption. This upsurge in power directly results in a substantial elevation in EMF exposure for users of UPWD. A straightforward yet effective solution for mitigating EMF exposure lies in the utilization of Ambient Backscatter Communications (ABC) [11], [12]. ABC operates by reflecting Radio Frequency (RF) signals modulated by reflecting devices known as backscatter tags, thereby efficiently repurposing existing wireless transmissions between sender and receiver. Additionally, the application of Machine Learning (ML) algorithms has demonstrated a pivotal role in diminishing uplink EMF levels [13].

To the best of the authors' knowledge, none of the work available in the literature has focused on utilizing exposure Dose in conjunction with PD-NOMA and UAV to optimize the uplink level of EMF exposure in a multi-user environment. One of the closest works is by [14], where the authors propose a mechanism of tethered UAV to reduce the total EMF exposure using the composite exposure metric Exposure Index (EI), without incorporating the Dose metric. The contributions to the knowledge of this paper are summarized as follows:

- We develop an optimization problem aimed at minimizing overall EMF exposure in a PD-NOMA-based multi-user cellular network while ensuring compliance with QoS requirements. Our proposed system incorporates UAV alongside the Dose metric to assess EMF exposure, distinguishing our approach from existing state-of-the-art solutions.
- We employ k-medoids for clustering UPWD during resource allocation. The k-medoids offers low complexity, high robustness, and quicker convergence compared to k-means clustering [15]. The number of users per sub-carrier is determined using silhouette analysis. The UPWD within a cluster are assigned a sub-carrier while employing an EMF-aware power allocation strategy.
- We conduct Monte Carlo simulations to validate the performance of the proposed PD-NOMA framework, which is based on UAV technology and employs ML. We compared the performance of our method with a PD-NOMA EMF minimization framework that does not utilize UAV, as well as an OFDMA EMF minimization framework without UAV involvement. Our proposed methodology notably reduces EMF exposure compared to the relevant non-UAV-based schemes, achieving reductions of at least 89% when compared to [13].

The paper is organized as follows: Section II presents the system model and describes the problem formulation. Section III elaborates on our proposed framework for resource and power allocation, with consideration for awareness of EMF exposure. Section IV provides our performance analysis and compares it with current methodologies. Lastly, Section V summarizes and concludes our findings.

II. System Model

In Figure 1, we present a communication configuration designed for densely populated urban areas, focusing on a single-cell scenario where $\breve{F}$ users, each equipped with a single antenna, interact with a Base Station (BS) employing PD-NOMA. The available system bandwidth, denoted as $\breve{W}$, is partitioned into $\breve{Q}$ subcarriers, allowing multiple users to share the same subcarrier due to the NOMA strategy. Given the challenges posed by poor channel conditions in this densely populated urban setting, direct communication between the $\breve{F}$ users and the BS is unfeasible. To overcome this hurdle, we introduce a UAV positioned at a fixed altitude, labeled $\breve{Z}_{\text{NTN}}$, which serves as an intermediary for data transmission from the UPWD to the BS. Here, $\breve{g}_{\breve{f},\breve{q},\breve{n}}$ represents the channel gain of user $\breve{f}$ over subcarrier $\breve{q}$ at time slot $\breve{n}$, accounting for both path loss and fading effects, and is expressed mathematically as follows:

$$\breve{g}_{\breve{f},\breve{q},\breve{n}} = \frac{\breve{\beta}_o |\breve{h}_{\breve{f},\breve{q},\breve{n}}|}{\breve{d}_{\breve{f}}^2}, \tag{1}$$

here, $\breve{\beta}_o$ denotes the channel gain power at a reference distance of one meter, $\breve{h}_{\breve{f},\breve{q},\breve{n}}$ represents the fading coefficient, and $\breve{d}_{\breve{f}}$ signifies the distance between the UAV and the $\breve{f}^{th}$ device. The term $\breve{d}_{\breve{f}}^2$ is defined as:

$$\breve{d}_{\breve{f}}^2 = \left[(\breve{X}_{\breve{f}} - \breve{X}_{\text{NTN}})^2 + (\breve{Y}_{\breve{f}} - \breve{Y}_{\text{NTN}})^2 + (\breve{Z}_{\text{NTN}})^2 \right]. \tag{2}$$

In this context, $\breve{X}$ and $\breve{Y}$ represent the x-coordinate and the y-coordinate of the positions of the UAV and UPWD, respectively. If $\breve{F}_{\breve{q},\breve{n}}$ users are assigned to the $\breve{q}^{\text{th}}$ subcarrier during time slot $\breve{n}$, the corresponding received signal at the UAV can be expressed as follows:

$$\breve{y}_{\breve{q},\breve{n}} = \sum_{\breve{f}=1}^{\breve{F}_{\breve{q},\breve{n}}} \sqrt{\breve{p}_{\breve{f},\breve{q},\breve{n}} \breve{g}_{\breve{f},\breve{q},\breve{n}}} \breve{x}_{\breve{f},\breve{q},\breve{n}} + \breve{z}_{\breve{q},\breve{n}}, \tag{3}$$

in this scenario, $\breve{x}_{\breve{f},\breve{q},\breve{n}}$ denotes the information signal of the $\breve{f}^{\text{th}}$ UPWD in an underlay PD-NOMA system, transmitted on subcarrier $\breve{q}$ at time slot $\breve{n}$. Similarly, $\breve{p}_{\breve{f},\breve{q},\breve{n}}$ represents the transmit power of the $\breve{f}^{\text{th}}$ UPWD at time slot $\breve{n}$ on the subcarrier $\breve{q}$, and $\breve{g}_{\breve{f},\breve{q},\breve{n}}$ symbolizes the channel gain between the $\breve{f}^{\text{th}}$ UPWD and the UAV at time slot $\breve{n}$ on the subcarrier $\breve{q}$. Additionally, $\breve{z}_{\breve{q},\breve{n}}$ characterizes the Additive White Gaussian Noise (AWGN) on subcarrier $\breve{q}$ at time slot $\breve{n}$, with zero mean and variance $\breve{\sigma}^2$. Interference arises due to the potential multiplexing of data from multiple users on the same subcarrier in NOMA. In a broader context, the cumulative interference encountered by the $\breve{f}^{\text{th}}$ user on the subcarrier $\breve{q}$ can be expressed as:

$$\breve{\bar{I}}_{\breve{f},\breve{q},\breve{n}} = \sum_{\breve{l}=1,\breve{l}\neq\breve{f}}^{\breve{F}_{\breve{q},\breve{n}}} \breve{p}_{\breve{l},\breve{q},\breve{n}} \breve{g}_{\breve{l},\breve{q},\breve{n}}. \tag{4}$$

At the receiver end in PD-NOMA, the Successive Interference Cancellation (SIC) technique is commonly employed to decipher the data streams of multiple users multiplexed together. Drawing from the principles of Multiple Input Multiple Output (MIMO) detection, where SIC originated [16], it is well understood that the sequence of detection plays a crucial role in performance. In SIC-enabled MIMO detection, data transmitted over the strongest channel links are typically decoded first, while those over the weakest links are processed last. Translating this concept to the uplink of PD-NOMA, it means that the user with the highest received power at the receiver, represented by $\breve{p}_{\breve{\pi}(1),\breve{q},\breve{n}} \breve{g}_{\breve{\pi}(1),\breve{q},\breve{n}}$, is decoded first. Conversely, the user with the lowest received power, denoted by $\breve{p}_{\breve{\pi}(\breve{F}_{\breve{q},\breve{n}}),\breve{q},\breve{n}} \breve{g}_{\breve{\pi}(\breve{F}_{\breve{q},\breve{n}}),\breve{q},\breve{n}}$, undergoes decoding last. In this context, $\breve{\pi}$ denotes a vector that permutes indices according to the SIC decoding sequence. Consequently, the power issuance strategy at the UPWD impacts the efficacy of the SIC process, i.e., its capability to disentangle the signals from different users. The multiplexing approach of PD-NOMA relies on the assumption that SIC can effectively decode the multiplexed signal [17], [18]. To incorporate this consideration into our model, we assert that successful decoding for any user $\breve{f}$ on subcarrier $\breve{q}$ at time slot $\breve{n}$ occurs when its received signal-to-residual interference ratio exceeds or equals a predefined threshold $\breve{\zeta}$, expressed as:

$$\breve{p}_{\breve{f},\breve{q},\breve{n}} \breve{g}_{\breve{f},\breve{q},\breve{n}} / \breve{I}_{\breve{f},\breve{q},\breve{n}} \geq \breve{\zeta}, \tag{5}$$

$\breve{\zeta} \geq 1$, where:

$$\breve{I}_{\breve{f},\breve{q},\breve{n}} = \sum_{\breve{l}=\breve{\pi}^{-1}(\breve{f})+1}^{\breve{F}_{\breve{q},\breve{n}}} \breve{p}_{\breve{\pi}(\breve{l}),\breve{q},\breve{n}} \breve{g}_{\breve{\pi}(\breve{l}),\breve{q},\breve{n}}. \tag{6}$$

In (6), $\breve{\pi}^{-1}(\breve{f})$ provides the position of $\breve{f}$ within the permutation vector $\breve{\pi}$. For example, if $\breve{\pi}(1) = 5$, then $\breve{\pi}^{-1}(5) = 1$, indicating that the index of 5 in $\breve{\pi}$ is 1. Therefore, the SIC process consistently achieves success, such that $\breve{I}_{\breve{\pi}(\breve{F}_{\breve{q},\breve{n}})} = 0, \forall \breve{q}, \breve{n}$. The total quantity of bits transmitted by the user $\breve{f}$ on the subcarrier $\breve{q}$ over a time slot $\breve{n}$ within a period $\breve{\tau}$ can be approximated using the following formula, which relies on equations (3), (6), and Shannon theory:

$$\breve{b}_{\breve{f},\breve{q},\breve{n}(\breve{\boldsymbol{\alpha}},\breve{\mathbf{p}})} = \breve{w}\breve{\tau}\,\breve{\alpha}_{\breve{f},\breve{q},\breve{n}} \log_2\left(1 + \frac{\breve{p}_{\breve{f},\breve{q},\breve{n}}\breve{g}_{\breve{f},\breve{q},\breve{n}}}{\breve{\sigma}^2 + \breve{I}_{\breve{f},\breve{q},\breve{n}}}\right), \tag{7}$$

in this context, $\breve{w} = \breve{W}/\breve{Q}$ denotes the bandwidth assigned to each subcarrier. The parameter $\breve{\alpha}_{\breve{f},\breve{q},\breve{n}}$ serves as a subcarrier allocation indicator, taking the value $\breve{\alpha}_{\breve{f},\breve{q},\breve{n}} = 1$ if the user $\breve{f}$ is assigned to the subcarrier $\breve{q}$ during time slot $\breve{n}$, and 0 otherwise. The $\breve{\mathbf{p}}$ encompasses transmit powers for all users, at all subcarriers, and all time slots. Similarly, $\breve{\boldsymbol{\alpha}}$ represents the subcarrier allocation status across different users, subcarriers, and time slots.

Regarding the individual user exposure in the uplink, its characterization can be articulated following the insights presented in [19], as:

$$\breve{E}_{\breve{f}}(\breve{\boldsymbol{\alpha}}, \breve{\mathbf{p}}) = \frac{\mathrm{SAR}_{\breve{f}}}{\breve{N}\breve{P}^{\mathrm{ref}}}\breve{\tau}\left(\overline{\breve{p}}_{\breve{f}}(\breve{N}) + \sum_{\breve{n}=1}^{\breve{N}}\sum_{\breve{q}=1}^{\breve{Q}} \breve{\alpha}_{\breve{f},\breve{q},\breve{n}}\breve{p}_{\breve{f},\breve{q},\breve{n}}\right); \tag{8}$$

in this context, $\breve{N}$ indicates the total number of time slots, and $\breve{P}^{\mathrm{ref}}$ signifies the reference incident power used to evaluate the Specific Absorption Rate (SAR) of the $\breve{f}^{\mathrm{th}}$ UPWD. The SAR metric is commonly used to assess EMF exposure from UPWD systems operating below 10 GHz. SAR measurements can be classified into average SAR or organ-specific SAR, such as those for the head or hand [3], [20]. Typically, SAR is expressed as:

$$\mathrm{SAR} = \frac{\breve{\Gamma} \times \breve{E}_{\breve{v}}^2}{\breve{M}_d} \quad \text{(W/kg)}. \tag{9}$$

In (9), $\breve{M}_d$ and $\breve{\Gamma}$ represent the mass density of the defined object or tissues and conductivity, respectively, while $\breve{E}_{\breve{v}}$ denotes the electric field. Additionally, $\overline{\breve{p}}_{\breve{f}}(\breve{N})$ in (8) signifies the signaling power used to facilitate the transmission of data of each UPWD relying on the total available time slots [21].

A. Problem Formulation

Our key aim is to create a scheduling technique that prioritizes EMF-awareness, with the goal of lowering exposure levels while also factoring in QoS requirements and utilizing PD-NOMA with SIC. To realize this objective, we initiate by delineating the mathematical structure of this approach through an optimization problem, outlined as follows:

$$\underset{\breve{\mathbf{p}},\breve{\boldsymbol{\alpha}}}{\text{minimize}} \quad \breve{E}(\breve{\boldsymbol{\alpha}}, \breve{\mathbf{p}}) = \quad \sum_{\breve{f}=1}^{\breve{F}} \breve{E}_{\breve{f}}(\breve{\boldsymbol{\alpha}}, \breve{\mathbf{p}}), \tag{10}$$

subject to:

$$\tilde{C}_A: \sum_{\breve{n}=1}^{\breve{N}}\sum_{\breve{q}=1}^{\breve{Q}} \breve{b}_{\breve{f},\breve{q},\breve{n}}(\breve{\boldsymbol{\alpha}}, \breve{\mathbf{p}}) = \breve{B}r_{\breve{f}}, \forall \breve{f}, \tag{11a}$$

$$\tilde{C}_B: \sum_{\breve{q}=1}^{\breve{Q}} \alpha_{\breve{f},\breve{q},\breve{n}}\breve{p}_{\breve{f},\breve{q},\breve{n}} \le \breve{P}_{\breve{f}}^{\max} \quad \forall \breve{f}, \forall \breve{n}, \tag{11b}$$

$$\tilde{C}_C: \breve{\alpha}_{\breve{f},\breve{q},\breve{n}}(\breve{p}_{\breve{f},\breve{q},\breve{n}}\breve{g}_{\breve{f},\breve{q},\breve{n}}/\breve{I}_{\breve{f},\breve{q},\breve{n}}) \ge \breve{\zeta} \quad \forall \breve{f}, \forall \breve{q}, \forall \breve{n}, \tag{11c}$$

$$\tilde{C}_D: \sum_{\breve{f}=1}^{\breve{F}} \breve{\alpha}_{\breve{f},\breve{q},\breve{n}} \le \breve{F}_{\breve{q},\breve{n}} \quad \forall \breve{q}, \forall \breve{n}. \tag{11d}$$

In equation (10), the function $\breve{E}(\breve{\boldsymbol{\alpha}}, \breve{\mathbf{p}})$ represents the collective uplink exposure encountered by the $\breve{F}$ users of the system over the $\breve{N}$ time slots. Simultaneously, the constraints outlined in equation (10) take the following form:

1) The constraint denoted by $\tilde{C}_A$ serves as a QoS parameter, ensuring that each user transmits the required number of bits, denoted as $\breve{B}r_{\breve{f}}$, in the prescribed sequence.

2) $\tilde{C}_B$ represents a constraint on transmit power, indicating that the transmit power of each UPWD is bounded by a maximum value, denoted as $\breve{P}_{\breve{f}}^{\max}$ for each time slot.
3) The constraint denoted by $\tilde{C}_C$ is associated with the SIC process at the receiver; when condition (11c) is satisfied, the SIC mechanism can eliminate certain interference from the received signal of user $\breve{f}$.
4) The constraint denoted by $\tilde{C}_D$ pertains to NOMA, indicating that in NOMA scenarios, the maximum number of users that can be assembled on the subcarrier $\breve{q}$ at any given time slot $\breve{n}$ is restricted to $\breve{F}_{\breve{q},\breve{n}}$.

Our optimization problem, delineated in (10) and (11), exhibits non-convexity owing to the binary nature of $\breve{\alpha}_{\breve{f},\breve{q},\breve{n}}$ [22] and the non-affine equality constraint $\tilde{C}_A$. To address this challenge effectively, we must initially alleviate its binary characteristic through a standard relaxation procedure. Following a similar approach as described in [23], we investigate sequential subcarrier and power assignments, wherein we first determine $\breve{\boldsymbol{\alpha}}$ with a fixed $\breve{\mathbf{p}}$ and subsequently optimize $\breve{\mathbf{p}}$ with a fixed $\breve{\boldsymbol{\alpha}}$. Furthermore, an adjustment of variables is necessary in (10) and (11) to convert $\tilde{C}_A$ into a convex form when $\breve{\boldsymbol{\alpha}}$ is fixed. These aspects are explored in more detail in the subsequent sections.

As highlighted in [13], it is crucial to note that we assume that the receiver can predict the Channel State Information (CSI) for the $\breve{F}$ users over $\breve{N}$ time slots ahead of time by utilizing uplink pilot signals.

III. Proposed EMF-aware UAV-assisted Solution

We present a two-step approach that integrates ML for sub-carrier assignment and an iterative strategy for power allocation. Through ML assistance, sub-carriers are allocated to an optimal number of users to minimize interference. The power allocation scheme in PD-NOMA guarantees efficient information decoding at the receiver, while adhering to QoS standards.

A. ML backed Subcarrier Allocation Strategy

The implementation of the PD-NOMA strategy enhances the spectral efficiency of communication systems [24] through the adept demultiplexing of multiple users sharing a common subcarrier, prioritizing based on their individual power reception levels. The effectiveness of this approach hinges largely on the receiver's capability to discern varying levels of received power among users, which in turn relies on judicious selection and grouping of users for multiplexing. Thus, in the uplink of cellular systems, user grouping can leverage spatial information to optimize performance. In the context of user grouping, the utilization of ML algorithms reduces complexity and improves the probability of converging towards an optimal solution, as demonstrated in comparison to non-ML methodologies [25], [26].

We utilize a k-medoids-based clustering technique to group $\breve{F}_{\breve{q},\breve{n}}$ users assigned to a sub-carrier $\breve{q}$ within time slot $\breve{n}$. Our investigation reveals that k-medoids outperform k-means in terms of clustering efficacy, offering lower time complexity and greater robustness [15]. To find out the favorable number of clusters efficiently, we employ Silhouette analysis. This method evaluates inter-cluster distances, aiding in the identification of an ideal number of clusters without requiring training on a dataset. In comparison to the elbow method utilized in previous work [13], Silhouette analysis demonstrates superior robustness and accuracy. Silhouette analysis calculates Silhouette coefficients, which reflect the distances of individual samples from their respective clusters. These coefficients range from $[-1, 1]$, with a score of 1 indicating significant distance from other clusters and -1 suggesting improper sample grouping. Consequently, the optimal number of clusters is determined when the average Silhouette coefficient, known as the Silhouette score, approaches 1.

After determining a sufficient value of the total number of clusters, denoted as $\breve{M}$, for a specific subcarrier, labeled as $\breve{q}$, at time slot $\breve{n}$, one user from each cluster is designated to utilize this subcarrier/time slot, following the guidelines outlined in Algorithm 1. Consequently, the count of users clustered on this particular subcarrier/time slot becomes $\breve{F}_{\breve{q},\breve{n}} = \breve{M}$. The normalized channel gain, in Algorithm 1, denoted as $\breve{G}_{\breve{f},\breve{q},\breve{n}}$, is employed for subcarrier allocation. This choice of utilizing $\breve{G}_{\breve{f},\breve{q},\breve{n}}$ instead of $\breve{g}_{\breve{f},\breve{q},\breve{n}}$ ensures fairness among users and mitigates EMF exposure by averting the allocation of the poorest subcarrier to any user during the given time slot $\breve{n}$. Additionally, $\breve{S}_{\breve{f}}$ denotes the quantity of assigned subcarriers per user.

B. Power Assignment

After performing the user grouping and subcarrier allocation procedures outlined in Section III-A, it becomes necessary to determine the appropriate transmit power levels for each user to mitigate uplink exposure to EMF. As detailed in Section II-2, even with the knowledge of $\breve{\alpha}$ obtained from the subcarrier allocation process, the optimization problem in equations (10) and (11) remains non-convex due to the non-linearity of constraint (11a). To address this, a variable transformation is employed:

$$\breve{p}_{\breve{f},\breve{q},\breve{n}} = \frac{(2^{\breve{r}_{\breve{f},\breve{q},\breve{n}}} - 1)(\sigma^2 + \breve{I}_{\breve{f},\breve{q},\breve{n}})}{\breve{g}_{\breve{f},\breve{q},\breve{n}}}, \tag{12}$$

by replacing $\breve{p}_{\breve{f},\breve{q},\breve{n}}$ with the expression provided in equation (12) within equations (10) and (11), the optimization problem can be reformulated as follows:

Algorithm 1: ML-driven sub-carrier allocation with UAV assistance.

INPUT ($\breve{g}_{\breve{f},\breve{q},\breve{n}}$, $\breve{N}$, $\breve{F}$, $\breve{Q}$,)
Stage 1:
Fix the value of $\breve{\boldsymbol{\alpha}} = \mathbf{0}$;
Fix the value of $\breve{G}_{\breve{f},\breve{q},\breve{n}} = \breve{g}_{\breve{f},\breve{q},\breve{n}}/\bar{\breve{g}}_{\breve{f}}$ $\forall \breve{f}, \breve{q}, \breve{n}$, $\bar{\breve{g}}_{\breve{f}} = \sum_{\breve{n}=1}^{\breve{N}} \sum_{\breve{q}=1}^{\breve{Q}} \breve{g}_{\breve{f},\breve{q},\breve{n}}/\breve{F}/\breve{N}$;
Stage 2:
for $M = 2 : F-1$ **do**
  Utilize k-medoids to perform clustering of $\breve{\mathbf{g}}_{\breve{q},\breve{n}}$ into $\breve{M}$ clusters $\forall \breve{f}, \breve{q}$;
end for
Estimate the value of $\breve{M}$ utilizing Silhouette mechanism;
Fix the value of $\breve{F}_{\breve{q},\breve{n}} = \breve{M}$ $\forall \breve{f}, \breve{q}$;
Fix the value of $\breve{S}_{\breve{f}} = \lfloor \sum_{\breve{q}=1}^{\breve{Q}} \sum_{\breve{n}=1}^{\breve{N}} \breve{F}_{\breve{q},\breve{n}}/\breve{F} \rfloor, \forall \breve{f}$.
Stage 3:
Use $\breve{G}_{\breve{f},\breve{q},\breve{n}}$ to perform subcarrier assignment.
From each cluster select the UPWD with maximum of $\breve{G}_{.,\breve{q},\breve{n}}$
Allocate $\breve{S}_{\breve{f}}$ sub-carrier to $\breve{F}$.
OUTPUT $\breve{\boldsymbol{\alpha}}$, $\breve{\boldsymbol{S}}$

$$\min_{\breve{\mathbf{r}}} \frac{\breve{\tau}}{\breve{N}} \sum_{\breve{f}=1}^{\breve{F}} \left(\bar{\breve{p}}_{\breve{f}}(\breve{N}) + \sum_{\breve{n}=1}^{\breve{N}} \sum_{\breve{q}=1}^{\breve{Q}} \frac{\breve{\alpha}_{\breve{f},\breve{q},\breve{n}} (2^{\breve{r}_{\breve{f},\breve{q},\breve{n}}} - 1)(\breve{\sigma}^2 + \breve{I}_{\breve{f},\breve{q},\breve{n}})}{\breve{g}_{\breve{f},\breve{q},\breve{n}}} \right), \tag{13}$$

subject to:

$$\begin{aligned}
&\tilde{C}_E : \breve{w}\breve{\tau} \sum_{\breve{n}=1}^{\breve{N}} \sum_{\breve{q}=1}^{\breve{Q}} \breve{\alpha}_{\breve{f},\breve{q},\breve{n}} \breve{r}_{\breve{f},\breve{q},\breve{n}} = \breve{B} r_{\breve{f}}, \\
&\tilde{C}_F : \sum_{\breve{q}=1}^{\breve{Q}} \frac{\breve{\alpha}_{\breve{f},\breve{q},\breve{n}} (2^{\breve{r}_{\breve{f},\breve{q},\breve{n}}} - 1)(\breve{\sigma}^2 + \breve{I}_{\breve{f},\breve{q},\breve{n}})}{\breve{g}_{\breve{f},\breve{q},\breve{n}}} \leq \breve{P}_{\breve{f}}^{\max}, \\
&\tilde{C}_G : \breve{\alpha}_{\breve{f},\breve{q},\breve{n}} ((2^{\breve{r}_{\breve{f},\breve{q},\breve{n}}} - 1)(\breve{\sigma}^2 + \breve{I}_{\breve{f},\breve{q},\breve{n}})/\breve{I}_{\breve{f},\breve{q},\breve{n}}) \geq \breve{\zeta},
\end{aligned} \tag{14}$$

the variable $\breve{r}_{\breve{f},\breve{q},\breve{n}}$, denoting the spectral efficiency of user $\breve{f}$ on subcarrier $\breve{q}$ at time slot $\breve{n}$, is defined as the ratio of $\breve{b}_{\breve{f},\breve{q},\breve{n}}$ to $(\breve{w}\breve{\tau})$. In contrast to equation (10), the constraint $\tilde{C}_E$ in equation (13) is expressed as an affine function of $\breve{\mathbf{r}}$. Furthermore, both the objective function and the constrained functions $\tilde{C}_F$ and $\tilde{C}_G$ in equation (13) are convex with respect to $\breve{\mathbf{r}}$, assuming $\breve{I}_{\breve{f},\breve{q},\breve{n}}$ is held constant. Thus, equation (13) presents a convex optimization problem, and its Lagrangian can be formally defined as:

$$\begin{aligned}
&\mathcal{L}(\breve{r}_{\breve{f},\breve{n}}, \breve{\lambda}_{\breve{f}}, \breve{\mu}_{\breve{f},\breve{n}}, \breve{\delta}_{\breve{f},\breve{q},\breve{n}}) = \\
&\frac{\breve{\tau}}{\breve{N}} \sum_{\breve{f}=1}^{\breve{F}} \left(\bar{\breve{p}}_{\breve{f}} + \sum_{\breve{n}=1}^{\breve{N}} \sum_{\breve{q}=1}^{\breve{Q}} \frac{\breve{\alpha}_{\breve{f},\breve{q},\breve{n}} (2^{\breve{r}_{\breve{f},\breve{q},\breve{n}}} - 1)(\breve{\sigma}^2 + \breve{I}_{\breve{f},\breve{q},\breve{n}})}{\breve{g}_{\breve{f},\breve{q},\breve{n}}} \right) \\
&+ \breve{\lambda}_{\breve{f}} (\breve{B} r_{\breve{f}} - \breve{w}\breve{\tau} \sum_{\breve{n}=1}^{\breve{N}} \sum_{\breve{q}=1}^{\breve{Q}} \breve{\alpha}_{\breve{f},\breve{q},\breve{n}} \breve{r}_{\breve{f},\breve{q},\breve{n}}) \\
&+ \breve{\mu}_{\breve{f},\breve{n}} \big(\breve{P}_{\breve{f}}^{\max} \breve{g}_{\breve{f},\breve{q},\breve{n}} - \sum_{\breve{q}=1}^{\breve{Q}} \breve{\alpha}_{\breve{f},\breve{q},\breve{n}} (2^{\breve{r}_{\breve{f},\breve{q},\breve{n}}} - 1)(\breve{\sigma}^2 + \breve{I}_{\breve{f},\breve{q},\breve{n}}) \big) \\
&+ \breve{\delta}_{\breve{f},\breve{q},\breve{n}} \breve{\alpha}_{\breve{f},\breve{q},\breve{n}} \left(\breve{\zeta} - (2^{\breve{r}_{\breve{f},\breve{q},\breve{n}}} - 1)(\breve{\sigma}^2 + \breve{I}_{\breve{f},\breve{q},\breve{n}})/\breve{I}_{\breve{f},\breve{q},\breve{n}} \right);
\end{aligned} \tag{15}$$

Algorithm 2: UAV-assisted iterative EMF-aware power optimization.

INPUT ($\breve{\boldsymbol{\alpha}}$, $\breve{\boldsymbol{S}}$, $\breve{F}$, $\breve{\zeta}$, $SAR_{\breve{f}}$, $\breve{P}_{\breve{f}}^{\max}$, $\breve{B}r_{\breve{f}}$, $\breve{\tau}$, $\overline{\breve{p}}_{\breve{f}}(\breve{N})$, $\breve{\sigma}^2$, $\breve{w}$)
Stage 1:
Set $\breve{p}_{\breve{f},\breve{q},\breve{n}}$=$\breve{P}_{\breve{f}}^{\max}/\breve{S}_{\breve{f}}$ $\forall \breve{f}$;
for $\breve{f}$ = 1 : $\breve{F}$ **do**
  Compute the initial value of $\breve{I}_{\breve{f},\breve{q},\breve{n}}$ utilizing (4) $\forall \breve{q}, \breve{n}$;
end for
Stage 2:
repeat
  for $\breve{f}$ = 1 : $\breve{F}$ **do**
    Compute $\breve{r}_{\breve{f},\breve{q},\breve{n}}$ using (15) employing iterative water-filling;
    Compute the updated value of $\breve{p}_{\breve{f},\breve{q},\breve{n}}$ utilizing (12);
    if $\breve{p}_{\breve{f},\breve{q},\breve{n}}\breve{g}_{\breve{f},\breve{q},\breve{n}}/\breve{I}_{\breve{f},\breve{q},\breve{n}} < \breve{\zeta}$ **then**
      Discover $\breve{r}_{\breve{f},\breve{q},\breve{n}}$ and $\breve{p}_{\breve{f},\breve{q},\breve{n}}$ such that $\breve{p}_{\breve{f},\breve{q},\breve{n}}\breve{g}_{\breve{f},\breve{q},\breve{n}}/\breve{I}_{\breve{f},\breve{q},\breve{n}} \geq \breve{\zeta}$;
    end if
    Compute the updated value of $\breve{I}_{\breve{f},\breve{q},\breve{n}}$ utilizing (6);
    Compute the value of $\breve{E}_{\breve{f}}$ utilizing (8);
  end for
until convergence
Stage 3:
Compute the value of $\breve{E}$ utilizing (10);
OUTPUT $\breve{E}$

in this context, the symbols, $\breve{\lambda}_{\breve{f}}$, $\breve{\mu}_{\breve{f},\breve{n}}$ and $\breve{\delta}_{\breve{f},\breve{q},\breve{n}}$ represent the Lagrange multipliers corresponding to the constraints $\tilde{C}_E$, $\tilde{C}_F$ and $\tilde{C}_G$, respectively.

Through the resolution of $\nabla\mathcal{L}(\breve{r}_{\breve{f},\breve{n}}, \breve{\lambda}_{\breve{f}}, \breve{\mu}_{\breve{f},\breve{n}}, \breve{\delta}_{\breve{f},\breve{q},\breve{n}}) = 0$, and the verification of adherence to all the Karush-Kuhn-Tucker (KKT) conditions [22], the outcome is as follows [13]:

$$\breve{r}_{\breve{f},\breve{q},\breve{n}} = \max\left(0, \log_2 \breve{\chi} + \log_2\left(\frac{\breve{w}\breve{g}_{\breve{f},\breve{q},\breve{n}}}{\ln(2)(\breve{\sigma}^2 + \breve{I}_{\breve{f},\breve{q},\breve{n}})}\right)\right), \tag{16}$$

in this context, the representation of $\breve{\chi}$ takes the form:

$$\breve{\chi} = \frac{\breve{\lambda}_{\breve{f}}^{\star}}{(1/\breve{N} - (\breve{\mu}_{\breve{f},\breve{n}}^{\star} + \breve{\delta}_{\breve{f},\breve{q},\breve{n}}^{\star}\breve{g}_{\breve{f},\breve{q},\breve{n}}/\breve{I}_{\breve{f},\breve{q},\breve{n}})/\breve{\tau})}. \tag{17}$$

Equation (17) represents a water-filling approach, amenable to analysis through iterative techniques like Secant and Newton-Raphson [27]. The power allocation process occurs in two stages. First, the transmit power of each user is precisely spread across its $\breve{S}_{\breve{f}}$ subcarriers, normalizing it relative to the maximum power of each UPWD. This initial distribution is then used to calculate interference levels among user groups that uses the same subcarrier. The interference is assessed using the SIC process, guided by a specified reference threshold $\breve{\zeta}$, as detailed in Section II. Notably, the SIC process prioritizes decoding users with superior channel gains first, assuming equal transmit power. Consequently, users with poorer channel conditions are considered interference-free if $\tilde{C}_G$ in equation (13), contingent upon $\breve{\zeta}$, is consistently satisfied.

Subsequently, iterative waterfilling is employed to refine the power levels of each $\breve{f}$ user sharing a subcarrier $\breve{q}$ while upholding both the QoS constraint $\breve{B}r_{\breve{f}}$ and the transmit power constraint $\breve{P}_{\breve{f}}^{\max}$. The power allocation must also adhere to constraint $\tilde{C}_G$; if not, recalibration is necessary. This two-stage process persists until convergence, signified by negligible changes in $\breve{p}_{\breve{f},\breve{q},\breve{n}}$ values between successive iterations. For further insights into the power allocation methodology, Algorithm 2 provides detailed guidance.

IV. Results and Discussions

In order to demonstrate the efficacy of the proposed framework for minimizing EMF while relying on UAV, PD-NOMA and ML technologies, we conduct a comprehensive evaluation of its performance and compare it with relevant state-of-the-art

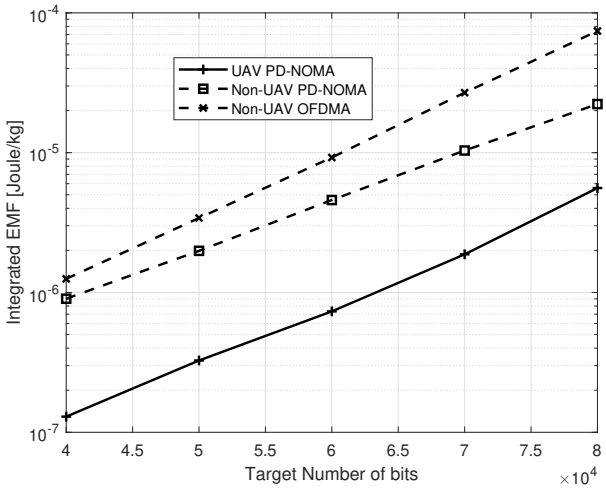

Figure 2: Integrated EMF exposure in the uplink direction, measured across a range of bit requirements (kbps).

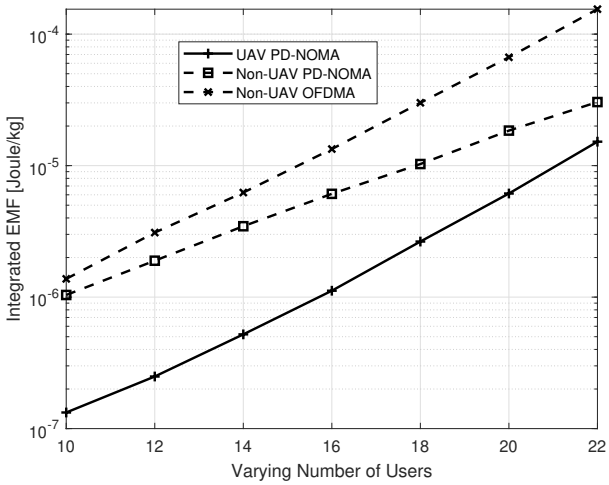

Figure 3: Integrated uplink EMF exposure with changing user counts.

approaches. The performance assessment was conducted by taking into account the following simulation assumptions and parameter values:

- To model propagation effects, we assume Rician fading and the path loss models used are defined in [28].
- The main simulation parameters are set with the following default values for the sake of simplicity and without the loss of generality: $\breve{Q} = 128$, $\breve{W} = 10$ MHz, $\breve{\tau} = 1$ ms, $\breve{F} = 15$, $\breve{N} = 10$, $\breve{P}^{\text{ref}} = 1$ Watt, $\breve{\sigma}^2 = -174$ dBm/Hz, $\breve{Z}_{\text{NTN}} = 100$ meters, $\text{SAR}_{\breve{f}} = 1$ W/kg, and $\breve{\zeta} = 1$.
- We have also made the assumption that all users possess an identical target number of required bits.

In Figure 2, we have conducted a performance comparison between our proposed UAV-assisted ML-enabled PD-NOMA scheme and two reference schemes: the non-UAV PD-NOMA scheme from [13] and the non-UAV OFDMA scheme from [29]. We gradually increased the required target number of bits while keeping the number of users fixed at 15, the number of time slots fixed at 10, and maintaining a constant number of subcarriers at 128. We observed a correlation between the increase in transmitted bits and the overall EMF exposure, attributed to the higher power demand for transmitting larger data volumes. Generally, PD-NOMA exhibited lower EMF exposure levels compared to OFDMA transmission due to its enhanced spectral efficiency, as discussed in [29]. However, when comparing the effectiveness of OFDMA and ML-based PD-NOMA from [13] with our proposed UAV-enabled PD-NOMA, we noted a significant decrease in EMF exposure, particularly when fewer bits were required. This reduction is attributed to the increased probability of LoS propagation facilitated by the UAV, resulting in improved channel conditions. At a fixed target number of bits (40 kbps), our proposed scheme demonstrated a substantial decrease in aggregated uplink EMF exposure compared to the approaches presented in [29] and [13], with reductions of 89% and 85%, respectively, as illustrated in Figure 2.

The illustration in Figure 3 presents a comparative analysis between the proposed method and the methodologies outlined

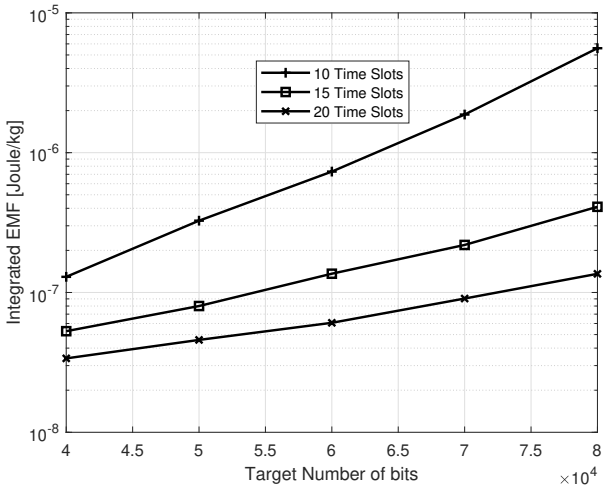

Figure 4: Integrated EMF levels across various time slots within the proposed framework employing UAV assisted PD-NOMA based ML technology.

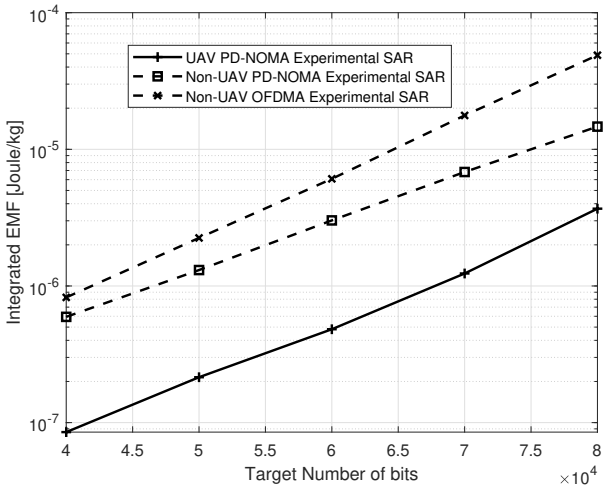

Figure 5: Integrated uplink EMF exposure at different levels of required bits for experimentally determined SAR values.

in [29] and [13]. This comparison is conducted under consistent conditions, maintaining a fixed number of sub-carriers at 128 and required target number are set to 60 kbps over 10 time slots, with varying user counts. The accumulation of EMF exposure intensifies with an increase in the number of users, leading to noticeable escalations in EMF exposure as user number rise. This escalation correlates with the necessity for higher transmit power per user to sustain consistent bit rates. Such trends persist even with constant allocations of sub-carriers and transmission window sizes. Notably, the proposed method exhibits significant performance enhancements compared to [29] and [13]. This improvement is attributed to the inclusion of a UAV, which enhances channel conditions by increasing the probability of LoS between users and the receiver.

To further affirm the effectiveness of the proposed approach, which combines UAV assistance, PD-NOMA methodology, and ML, we delve into its performance across a range of target bit counts. This examination is conducted under various fixed time slot durations, denoted by $\breve{N}$ values of 10, 20, and 30, as illustrated in Figure 4. The analysis reveals a significant finding: as the transmission duration extends, there is a discernible decrease in EMF exposure, all while maintaining a steady $\breve{B}r$ value. This implies that despite the increase in $\breve{B}r$, the overall accumulation of EMF exposure reduces over time, which signifies the importance of using Dose metric to optimize the EMF exposure by exploiting time domain.

Similarly to the study conducted by [13], in Figure 5, we explore the effects of varying the target bit count on the total uplink EMF exposure for a fixed number of users and time slots, utilizing experimentally determined SAR values. The SAR value utilized in Figure 5 is 0.658545 W/kg, which corresponds to the SAR value determined experimentally for cheek positioning as detailed in [13], using the IEEE/IEC 62704-1 averaging method. As depicted in Figure 5, the aggregate EMF exposure is reduced with the incorporation of UAV compared to scenarios without UAV in both OFDMA and PD-NOMA systems. This confirms the efficacy of the methodology employed in the proposed framework.

V. Conclusion

In this paper, we demonstrate for the first time that the joint utilization of UAV and the exposure Dose metric can effectively optimize uplink EMF exposure levels. We have devised a two-stage allocation strategy to decouple the non-convex problem. The ML technique is used for resource allocation, while power allocation is accomplished using iterative methods. Compared to similar non-UAV-based techniques, the proposed utilization of UAV can reduce uplink EMF exposure levels by at least 89%, particularly in dense urban scenarios. In future work, we aim to expand our research by exploring multi-cell scenarios. Enhancing the practicality and resilience of our methods will be a key focus, as we plan to incorporate considerations of interference from neighboring cells into the design.

Acknowledgment

This work was funded by the Deanship of Graduate Studies and Scientific Research at Jouf University under grant No. (DGSSR-2024-02-01103) and this research was supported in part by Basic Science Research Program through the National Research Foundation of Korea (NRF) funded by the Ministry of Education (NRF-2021R1A6A1A03039493) and in part by the NRF Grant funded by the Korea government (MSIT)(NRF-2022R1A2C1004401).

Author contributions: CRediT

Muhammad Ali Jamshed: Conceptualization; Formal analysis; Software; Methodology; Visualization; Writing – original draft; Writing – review & editing. **Ali Nauman:** Formal analysis; Methodology; Writing – review & editing. **Ayman A. Althuwayb:** Conceptualization; Investigation; Methodology; Project administration; Supervision; Writing – review & editing. **Sung Won Kim:** Conceptualization; Investigation; Methodology; Project administration; Supervision.

References

[1] M. A. Jamshed, K. Ali, Q. H. Abbasi, M. A. Imran, and M. Ur-Rehman, "Challenges, applications, and future of wireless sensors in internet of things: A review," *IEEE Sensors Journal*, vol. 22, no. 6, pp. 5482–5494, 2022.

[2] M. U. Rehman and M. A. Jamshed, "Low electromagnetic field exposure wireless devices: Fundamentals and recent advances," 2022.

[3] M. A. Jamshed, F. Heliot, and T. W. Brown, "A survey on electromagnetic risk assessment and evaluation mechanism for future wireless communication systems," *IEEE Journal of Electromagnetics, RF and Microwaves in Medicine and Biology*, vol. 4, no. 1, pp. 24–36, 2019.

[4] M. A. Jamshed, A. Kaushik, M. Toka, W. Shin, M. Z. Shakir, S. P. Dash, and D. Dardari, "Synergizing airborne non-terrestrial networks and reconfigurable intelligent surfaces-aided 6g iot," *IEEE Internet of Things Magazine*, vol. 7, no. 2, pp. 46–52, 2024.

[5] A. Guerra, D. Dardari, and P. M. Djuric, "Dynamic radar networks of UAVs: A tutorial overview and tracking performance comparison with terrestrial radar networks," *IEEE Vehicular Technology Magazine*, vol. 15, no. 2, pp. 113–120, 2020.

[6] M. A. Jamshed, A. Kaushik, A. G. Armada, M. Di Renzo, D. Lee, R. Senanayake, and O. A. Dobre, "Guest editorial: Technical advancements in ntn-assisted internet-of-things: Global connectivity from the sky," *IEEE Internet of Things Magazine*, vol. 7, no. 1, pp. 10–11, 2024.

[7] L. Dai, B. Wang, Z. Ding, Z. Wang, S. Chen, and L. Hanzo, "A survey of non-orthogonal multiple access for 5g," *IEEE communications surveys & tutorials*, vol. 20, no. 3, pp. 2294–2323, 2018.

[8] M. Awais, H. Pervaiz, M. A. Jamshed, W. Yu, and Q. Ni, "Energy-aware resource optimization for improved urllc in multi-hop integrated aerial terrestrial networks," *IEEE Transactions on Green Communications and Networking*, 2023.

[9] B. Makki, K. Chitti, A. Behravan, and M.-S. Alouini, "A survey of noma: Current status and open research challenges," *IEEE Open Journal of the Communications Society*, vol. 1, pp. 179–189, 2020.

[10] M. A. Jamshed, A. Nauman, M. A. B. Abbasi, and S. W. Kim, "Antenna selection and designing for thz applications: suitability and performance evaluation: a survey," *IEEE Access*, vol. 8, pp. 113 246–113 261, 2020.

[11] M. A. Jamshed, W. U. Khan, H. Pervaiz, M. A. Imran, and M. Ur-Rehman, "Emission-aware resource optimization framework for backscatter-enabled uplink noma networks," in *2022 IEEE 95th Vehicular Technology Conference:(VTC2022-Spring)*. IEEE, 2022, pp. 1–5.

[12] M. A. Jamshed, Y. A. Qadri, A. Nauman, and H. Jung, "Electromagnetic field exposure-aware ai framework for integrated sensing and communications-enabled ambient backscatter wireless networks," *IEEE Internet of Things Journal*, 2024.

[13] M. A. Jamshed, F. Heliot, and T. W. Brown, "Unsupervised learning based emission-aware uplink resource allocation scheme for non-orthogonal multiple access systems," *ieee transactions on vehicular technology*, vol. 70, no. 8, pp. 7681–7691, 2021.

[14] Z. Lou, A. Elzanaty, and M.-S. Alouini, "Green tethered uavs for emf-aware cellular networks," *IEEE Transactions on Green Communications and Networking*, vol. 5, no. 4, pp. 1697–1711, 2021.

[15] T. Velmurugan and T. Santhanam, "Computational complexity between K-means and K-medoids clustering algorithms for normal and uniform distributions of data points," *Journal of computer science*, vol. 6, no. 3, p. 363, 2010.

[16] G. D. Golden, C. Foschini, R. A. Valenzuela, and P. W. Wolniansky, "Detection algorithm and initial laboratory results using V-BLAST space-time communication architecture," *Electronics letters*, vol. 35, no. 1, pp. 14–16, 1999.

[17] W. U. Khan, M. A. Jamshed, E. Lagunas, S. Chatzinotas, X. Li, and B. Ottersten, "Energy efficiency optimization for backscatter enhanced noma cooperative v2x communications under imperfect csi," *IEEE Transactions on Intelligent Transportation Systems*, 2022.

[18] W. U. Khan, M. A. Jamshed, A. Mahmood, E. Lagunas, S. Chatzinotas, and B. Ottersten, "Backscatter-aided noma v2x communication under channel estimation errors," in *2022 IEEE 95th Vehicular Technology Conference:(VTC2022-Spring)*. IEEE, 2022, pp. 1–6.

[19] E. Conil, "D2. 4 Global wireless exposure metric definition v1," *LexNet project*, 2013.

[20] M. A. Jamshed, T. W. Brown, and F. Héliot, "Dual antenna coupling manipulation for low sar smartphone terminals in talk position," *IEEE transactions on antennas and propagation*, vol. 70, no. 6, pp. 4299–4306, 2022.

[21] 3GPP, "3GPP TS 36.213,'Evolved Universal Terrestrial Radio Access (E-UTRA); Physical layer procedures (Release 12)," 2015.

[22] Z.-Q. Luo and W. Yu, "An introduction to convex optimization for communications and signal processing," *IEEE Journal on selected areas in communications*, vol. 24, no. 8, pp. 1426–1438, 2006.

[23] M. Al-Imari, P. Xiao, M. A. Imran, and R. Tafazolli, "Low complexity subcarrier and power allocation algorithm for uplink OFDMA systems," *EURASIP Journal on Wireless Communications and Networking*, vol. 2013, no. 1, pp. 1–6, 2013.

[24] W. U. Khan, F. Jameel, M. A. Jamshed, H. Pervaiz, S. Khan, and J. Liu, "Efficient power allocation for noma-enabled iot networks in 6g era," *Physical Communication*, vol. 39, p. 101043, 2020.

[25] H. Ye, G. Y. Li, and B.-H. F. Juang, "Deep reinforcement learning based resource allocation for V2V communications," *IEEE Transactions on Vehicular Technology*, vol. 68, no. 4, pp. 3163–3173, 2019.
[26] A. Nauman, M. A. Jamshed, Y. A. Qadri, R. Ali, and S. W. Kim, "Reliability optimization in narrowband device-to-device communication for 5g and beyond-5g networks," *IEEE Access*, vol. 9, pp. 157 584–157 596, 2021.
[27] M. Abramowitz and I. Stegun, "Handbook of Mathematical Functions: With Formulas, Graphs, and Mathematical Tables Applied mathematics series," *National Bureau of Standards, Washington, DC*, 1964.
[28] J. Wu, S. Rangan, and H. Zhang, *Green communications: theoretical fundamentals, algorithms, and applications*. CRC press, 2016.
[29] Y. A. Sambo, M. Al-Imari, F. Héliot, and M. A. Imran, "Electromagnetic emission-aware schedulers for the uplink of OFDM wireless communication systems," *IEEE Transactions on Vehicular Technology*, vol. 66, no. 2, pp. 1313–1323, 2016.